*Article*

# Three-Dimensional Subsurface Model of Luk-Ulo Melange Complex, Karangsambung, Indonesia: Insights from Gravity Modeling

**Faridz Nizar Ahmady** [1,*] **, Djoko Santoso** [1,2] **, Susanti Alawiyah** [1] **and Asep Saepuloh** [3]

1   Faculty of Mining and Petroleum Engineering, Institut Teknologi Bandung, Jalan Ganesa 10, Bandung 40132, Indonesia; dsantoso78@yahoo.com (D.S.); susanti.alawiyah@itb.ac.id (S.A.)
2   Department of Petroleum Engineering, Institute Technology Science Bandung, Bekasi 17530, Indonesia
3   Faculty of Earth Sciences and Technology, Institut Teknologi Bandung, Jalan Ganesa 10, Bandung 40132, Indonesia; saepuloh@itb.ac.id
*   Correspondence: faridnyzer@itb.ac.id

**Abstract:** The Luk-Ulo Melange Complex (LMC) is characterized by a chaotic assemblage of mixed rocks with a block-in-matrix fabric. The exposed blocks consist of various scattered rock types, trending in an ENE-WSW direction. In the case of Mt. Parang, the origin of the diabase remains uncertain, with ongoing debate as to whether it is associated with in situ volcanic activity or represents an exotic block within the melange deposit. Subsurface data obtained through geophysical investigation can aid in modeling the geometry of intrusive bodies using inverse modeling techniques. In this study, we conducted a gravity survey and performed 3D inverse modeling to investigate the subsurface beneath Karangsambung. A total of 818 gravity data points and 28 rock density measurements were integrated with existing geological data to construct an a priori 3D geological model. To ensure the results align with geological concepts, the 3D inversion utilized a stochastic approach, allowing for the incorporation of multiple geological constraints over fifty million iterative procedures. Ultimately, the inversion successfully reduced the misfit between observed and calculated data from 2.71 to 0.55 mGal. Based on the inverted 3D model, the diabase rock in Mt. Parang is identified as having an intrusive origin. The intrusion model exhibited minimal changes in density, volume, and shape during the inversion process. Additionally, the model suggests the presence of a solidified magma reservoir at a depth of approximately 3 km, potentially related to Dakah volcanism. The inverted model also reveals the block-in-matrix structure of the Luk-Ulo Melange Complex in the northern area.

**Keywords:** gravity inversion; Karangsambung; gravity modeling; Luk-Ulo Melange Complex; subsurface geology

## 1. Introduction

There are only a limited number of locations on the island of Java where pre-Tertiary rocks can be observed and studied. One of them is in the Karangsambung sub-district in Central Java, where the Luk-Ulo Melange Complex (LMC) is exposed (Figure 1). The study of these pre-Tertiary rocks holds significant tectonic importance, as it provides valuable insights into the geological evolution of the region. The LMC provides evidence of tectonic evolution in southeastern Sundaland, particularly associated with the southward migration of the Indo-Australian plate's subduction beneath the Eurasian plate during the Cretaceous period [1–3]. Among the few locations in Java, Karangsambung stands out as the most suitable site for studying melange deposits linked to subduction processes. These deposits are characterized by a chaotic assemblage of mixed rocks exhibiting a block-in-matrix fabric [4,5]. The blocks consist of various rock types scattered in an ENE-WSW orientation and are embedded within a scaly clay matrix [5].
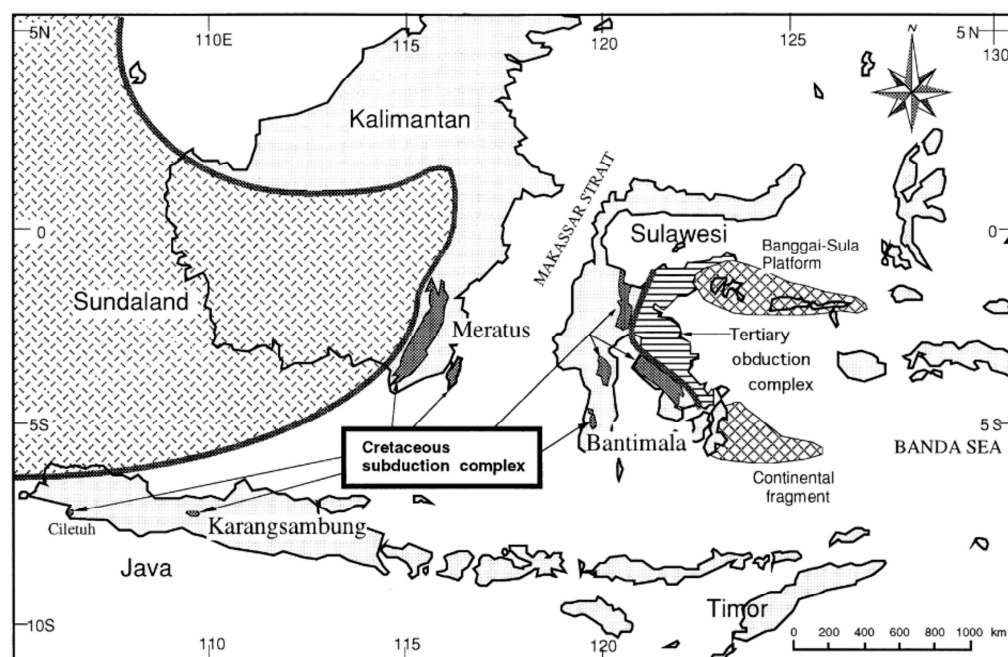
**Figure 1.** Distribution of Cretaceous subduction-related outcrops in Indonesia, adapted from Wakita et al. [6]. Most outcrops are located in Java, Kalimantan, and Sulawesi. The green rectangle indicates the study area.

A study by [7] highlighted the occurrence of submarine volcanic arcs within the LMC and introduced the Dakah volcanic unit, primarily consisting of basalt and diabase outcrops at Mt. Parang and Dakah. This diabase apparently cuts through olisostromal deposits of Karangsambung and Totogan formations. Later, Setiawan et al. [8] proposed the Dakah volcanism concept, interpreting the diabase outcrops at Mt. Parang as a volcanic neck, with an estimated central eruption located in Dakah village. K-Ar dating of the diabase outcrops yielded ages ranging from 39.9 to 26.5 Ma [9]. In contrast, nannoplankton dating of the Totogan Formation suggested a younger age ($\pm$36 Ma to $\pm$20.5 Ma, NP18-NN2) than the K-Ar dating [10]. This discrepancy introduces ambiguity into the volcanic interpretation, as younger rocks typically cut through older formations. Additionally, the dating inconsistency raises the possibility that the scattered diabase outcrops within the olisostromal deposits could be considered blocks transported from their original locations, forming part of the sedimentary melange deposit. The existing interpretation, based solely on surface geological evidence and dating, is insufficient to determine the origin of the diabase in Karangsambung. Subsurface data obtained through geophysical methods are necessary to accurately understand the geometry of the underlying rocks. Therefore, it is essential to integrate geophysical surveys with surface data to fully assess the origin and geometric characteristics of the diabase.

Subsurface data derived from geophysical surveys are crucial for determining the geometry of volcanic and intrusive bodies, such as dikes, sills, stocks, and batholiths [11–13]. Moreover, geophysical approaches provide valuable insights into the lateral distribution of blocks within the melange environment, particularly in tropical areas where weathering processes are extensive. A regional seismic tomography survey in Central Java indicated the presence of accreted continental fragments, related to the tectonic collision between the East Java microcontinent and Sundaland [14]. Previous gravity and magnetic surveys in Karangsambung have estimated subsurface models through 2D forward modeling (e.g., [15–17]), suggesting a possible diabase intrusion near Mt. Parang, as indicated by strong gravity and magnetic anomalies. Conversely, Laesanpura et al. [16] reported an intriguing result from 1D audio-magnetotelluric (AMT) inversion, which showed the discontinuity of the diabase at depth, potentially representing a sill. Later, Handayani et al. [18] explored this

idea further using 2D Electrical Resistivity Tomography (ERT) across the diabase outcrop at Mt. Parang to ascertain the origin of the volcanic rock. Their results suggested that the diabase body does not extend downward, which aligns with the findings of Laesanpura et al. [16]. Current geophysical approaches in Karangsambung, which predominantly rely on 1D and 2D modeling, require enhancement through the adoption of 3D geophysical modeling to improve structural interpretations. The application of 3D modeling based on geophysical data is critical, as it allows for a more comprehensive and detailed analysis of the geometry of the diabase at Mt. Parang.

The 3D modeling of subsurface structures requires an extensive data distribution for detailed interpretation. Karangsambung's complex morphology and dense vegetation make geophysical investigations challenging. Consequently, we have selected the gravity method as our primary geophysical tool. Gravity surveys are cost-effective compared to more complex geophysical approaches, such as seismic and electromagnetic surveys, and are widely employed to identify subsurface structures across various geological contexts, including melanges and melange complexes [19–22], the Alpine region [23], the Great Sumatran Fault [24,25], and the Sulawesi Ultramafic Belt [26]. The primary objectives of this study are to conduct gravity surveys and construct a robust 3D interpretation of the subsurface structure beneath Karangsambung by integrating geological and gravity data into a 3D inverse model.

## 2. Geological Setting

The study of tectonic evolution in the Java region, which includes the Luk-Ulo Melange Complex in Karangsambung, has been discussed in previous research [3,5,27–29]. The detailed geological map of Karangsambung is reported in Figure 2. The Luk Ulo Melange Complex (LMC) is the product of Late Cretaceous paleosubduction [30] and the subsequent collision between the East Java microcontinent and Sundaland [27,31]. Relative dating of radiolarian fossils found in chert and siliceous shale indicate that the age of the Luk-Ulo Melange Complex is Early to Late Cretaceous [30]. This pre-Tertiary melange is characterized by blocks embedded within a sheared shale matrix (scaly clay). These blocks consist of various rock types, including gabbro, serpentinite, schist, and chert, which have undergone low to high grade metamorphism [29,32,33]. The petrological study by Suparka [34] suggests that the dismembered ophiolite blocks within the LMC originated from mid-ocean ridge activities. These ophiolites were uplifted and exposed due to the Late Cretaceous paleosubduction of the Indo-Australian plate beneath the Eurasian plate. In the study area, the LMC is unconformably overlain by Tertiary sedimentary rocks, including the Karangsambung, Totogan, Waturanda, and Penosogan formations [35].
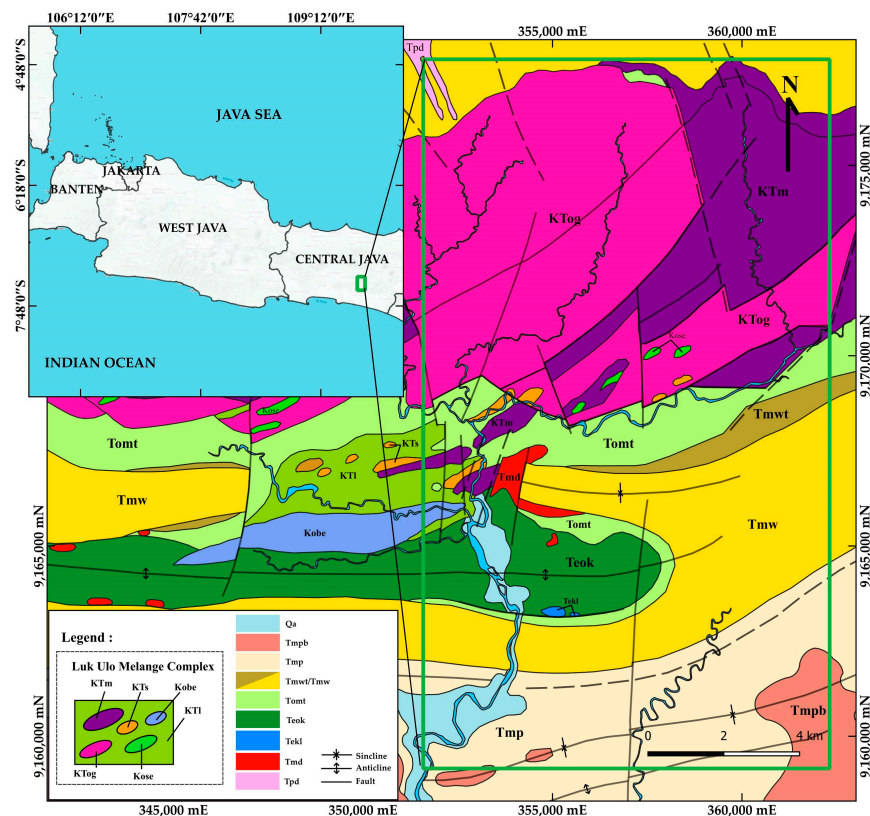
**Figure 2.** A geological map of Karangsambung, modified from Asikin et al. [35] and Condon et al. [36]. The southern region is primarily composed of Tertiary sedimentary rocks, including the Karangsambung Formation (Teok), isolated reef limestone (Tekl), Totogan Formation (Tomt), Waturanda Formation (Tmw/Tmwt), Penosogan Formation (Tmp), and Halang Formation (Tmpb), with a diabase intrusion (Tmd) cutting through the Karangsambung and Totogan formations. The northern region is dominated by the Luk-Ulo Melange Complex (LMC), featuring a block-in-matrix structure with basaltic pillow lava and radiolarian chert (Kobe), gabbro (KTog), metasediment/greywacke (KTs), schist/phyllite (KTm), and serpentinite (Kose) blocks embedded in a scaly clay matrix (KTl). Additionally, intrusive diorite (Tpd) is found in the upper region. The youngest deposits, Quaternary alluvium (Qa), are distributed near the river. The green rectangle indicates the boundary of the gravity survey area for this study.

The Karangsambung and Totogan formations share similar characteristics, notably the presence of olisostromal deposits [5]. Olisostrom is classified as a sedimentary melange, formed by gravitational mass movements occurring in front of accretionary wedges during the pre-collisional stage [4]. According to Kapid and Harsolumakso [10], the ages of the Karangsambung and Totogan formations are estimated to be in the middle to late Eocene and late Eocene to early Oligocene, respectively. In Mt. Parang, volcanic rock outcrops (diabase) are surrounded by these olisostromal deposits. A comprehensive geological study by Setiawan et al. [8] proposes the genesis of Dakah volcanism based on field surveys and petrological analysis of the diabase. Surface observations reveal a baking effect at the contact between the diabase and the Karangsambung Formation, suggesting an intrusive origin, likely as a dike or volcanic neck [8]. Additionally, petrological analysis identified secondary minerals such as natrolite, indicating that the volcanic activity may have occurred in a subsea environment [8]. K-Ar dating of two diabase samples from Karangsambung suggests that the Dakah volcanic event occurred in the late Eocene to early Oligocene [9].

However, Harsolumakso [37] presents a different interpretation of the diabase in Mt. Parang. Field observations indicate tectonic contacts between the scaly clay matrix, possibly part of the Karangsambung or Totogan Formation, and diabase outcrops in Kali Jebug. Such tectonic contacts are commonly observed in the block-matrix structures of melange

deposits [4]. Therefore, the scattered diabase in Karangsambung represents exotic blocks within the sedimentary melange (olisostromal deposits) that were transported from their original location [37].

Based on Asikin et al. [35], the Totogan Formation is conformably overlain by the Waturanda Formation, which consists of interbedded sandstone and breccia. The breccia contains fragments of volcanic basalt and andesite within a coarse sandstone matrix. The Waturanda Formation is conformably overlain by the Penosogan Formation, which is composed of interbedded marl and calcareous sandstone. The youngest formation in the study area is the Halang Formation, characterized by breccia and sandstone. In general, two structural patterns can be identified in Karangsambung. Harsolumakso and Noeradi [38] showed that the northern part, covering most of the Luk-Ulo Melange Complex, exhibits a structural pattern trending NNE-SSW, while the southern part features a structural pattern elongated in the E-W direction.

## 3. Data and Acquisition

A land gravity survey was conducted from July 2018 to October 2019 to measure gravity anomalies in the study area. A total of 818 gravity data points were measured, covering a $10 \times 18.8$ km$^2$ area in Karangsambung, with station spacing of approximately 250 m. The distribution of gravity stations is shown in Figure 3a. The measurement was carried out using Scintrex CG-5 Autograv (Scintrex Limited, Concord, ON, Canada). Following standard procedures, the gravimeter was calibrated and stabilized at least three days prior to measurement in order to ensure the accuracy of the gravity data. The survey also adopted a looping method to compute daily instrumental drift. At each station, at least three consecutive gravity readings were recorded, with a maximum deviation of 10 μGal among them. The positioning of each gravity station was recorded using two RTK-GPS (D-GPS) units.
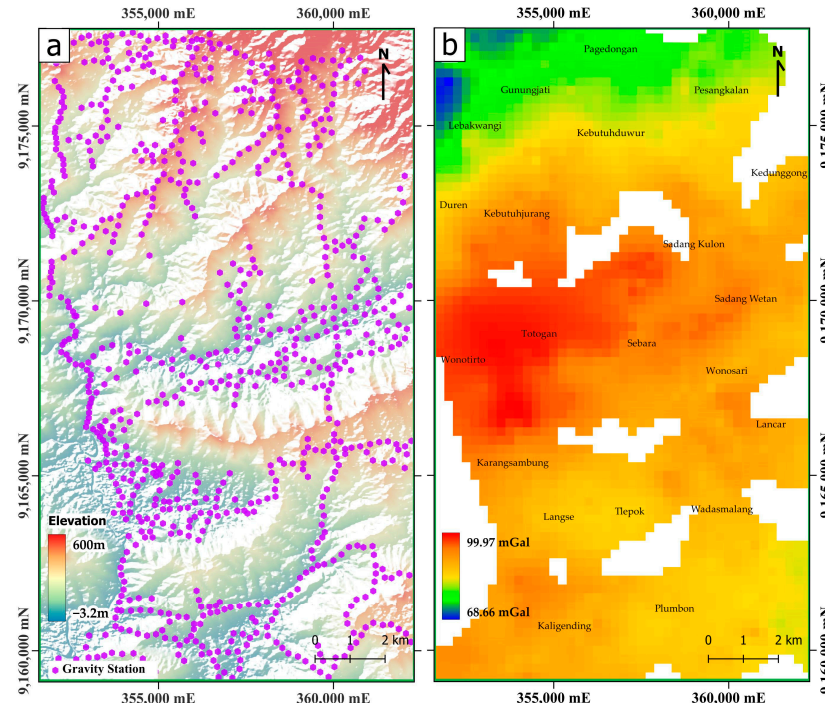


**Figure 3.** The distribution of the 818 gravity stations is represented by purple dots on the map, with the color bar indicating elevation levels, thus reflecting the morphological variation within the research area (**a**). The Complete Bouguer Anomaly (CBA) ranges from 68.66 to 99.97 mGal, with strong positive anomalies, depicted in orange to reddish tones, primarily concentrated in the central area. In contrast, the weakest anomalies, shown in green to bluish tones, are predominantly located in the upper regions (**b**).

Additionally, 28 rock samples were collected from various formations in Karangsambung during the gravity survey. The density of these rock samples was measured in the petrophysical laboratory, with a summary of the results listed in Table 1. The average density of the rock samples is approximately 2.61 g/cm$^3$. These measured densities are consistent with results from previous studies in adjacent areas, such as [39].

**Table 1.** The measured densities of twenty-eight rock samples from the Karangsambung area, optimized density, inverted density, volume changes after inversion, and density data from a previous study by Purwasatriya et al. [39].

| No | Rock Samples | N | Measured (g/cm$^3$) | Optimized (g/cm$^3$) | Inverted (g/cm$^3$) | Volume Changes * (%) | Information |
|----|--------------|---|---------------------|----------------------|---------------------|----------------------|-------------|
| 1 | Luk-Ulo Melange Complex | | | | - | - | |
| | a. Gabbro | 3 | 2.75–2.90 | - | - | - | |
| | b. Sarpentinite | 3 | 2.63–2.78 | - | - | - | |
| | c. Phyllite | 3 | 2.59–2.70 | - | - | - | |
| | d. Melange Matrix | 2 | 2.22–2.41 | 2.36 | 2.42 ± 0.053 | 1.54 | |
| | e. Melange Block 1 | | | 2.79 | 2.80 ± 0.060 | −0.24 | Optimized density is estimated according to the sample of gabbro |
| | f. Melange Block 2 | | | 2.65 | 2.70 ± 0.057 | −0.04 | Optimized density is estimated according to the sample of serpentinite |
| | g. Melange Block 3 | | | 2.66 | 2.69 ± 0.057 | −0.02 | Optimized density is estimated according to the sample of phyllite |
| | h. Basement | | - | 2.85 | 2.85 ± 0.050 | −1.64 | |
| 2 | Karangsambung Fm. | 2 | 2.30–2.40 | 2.37 | 2.42 ± 0.050 | 0.89 | |
| 3 | Totogan Fm. | 3 | 2.45–2.53 | 2.48 | 2.50 ± 0.070 | 0.19 | |
| 4 | Diabase | 4 | 2.68–2.85 | 2.78 | 2.77 ± 0.051 | −0.14 | |
| 5 | Waturanda Fm. | 3 | 2.40–2.68 | 2.63 | 2.62 ± 0.106 | −0.68 | |
| 6 | Panasogan Fm. | 2 | 2.42–2.56 | 2.48 | 2.35 ± 0.056 | 0.10 | |
| 7 | Halang Fm. | 2 | 2.55–2.65 | 2.62 | 2.49 ± 0.054 | 0.00 | |
| 8 | Halang Fm. | | 2.63–2.74 | | | | Purwasatriya et al. [39] |

* Volume changes were computed based on the changes in volume on specific formation before and after the inversion process.

All measured gravity data were corrected using standard gravity corrections [40] to obtain the observed anomaly. Tidal correction was automatically applied using the Longman [41] equation, which is integrated into the gravimeter. Instrumental drift was calculated manually, assuming linear drift during each looping survey. Bouguer corrections were applied to account for the gravitational attraction of the mass between the observation point and the reference level, yielding simple Bouguer Anomalies. The final correction, applied to obtain Complete Bouguer Anomalies (CBA), was the terrain correction. The terrain correction was calculated automatically and simultaneously by the computer using an exact formula for rectangular prisms [42,43]. To achieve this, the topography surrounding each station was discretized into several zones of prisms with increasing radii, extending up to 166.7 km. The gravity attraction of each prism was then calculated for each station. Each zone was associated with a different Digital Elevation Model (DEM) cell size, depending on the distance from the station. A detailed DEM with a resolution of 0.27 arcseconds (equivalent to 8 m), obtained from the Indonesian Geospatial and Informatic Department (BIG), was used to compute the inner terrain correction within 1 km of each station. Additionally, the regional terrain correction up to 166.7 km was computed using digital elevation data derived from SRTM30 DEM, downloaded from USGS. A reference density of 2.61 g/cm$^3$, comparable with the average density of the surface rock sample (Table 1) was used in Bouguer and terrain correction. In addition, the kriging method with

a radius of 250 m was employed to interpolate unavailable data in the surrounding area and to construct the Complete Bouguer Anomaly map (Figure 3b). The Complete Bouguer Anomaly ranges from 68.66 mGal to 99.97 mGal. The blank area represents regions outside the measurement area, generated during interpolation to prevent extrapolation of the data. The strongest gravity anomalies were observed near Mt. Parang, Wonotirto, and Totogan, while the weakest gravity anomalies were primarily observed in the upper region.

## 4. Methodology

### 4.1. Filtering of Gravity Data

In this study, our focus is on detecting shallow gravity anomalies, specifically those related to geological structures up to a depth of 4 km. These anomalies are typically characterized by short to medium wavelength signals in the gravity data. To isolate these signals, we developed a high-pass spectral filter based on the Butterworth filter. The Butterworth filter formula is given as follows:

$$H(k) = \frac{1}{1 + \left(\frac{k_c}{k}\right)^{2n}} \tag{1}$$

where $H(k)$ represents the filter response, $k$ denotes the frequency, $k_c$ is the cutoff frequency, and $n$ indicates the filter order, which controls the sharpness of the filter's transition [44]. In this study, we choose to use a filter order ($n$) = 8. Figure 4 shows the filter design implemented in this study.
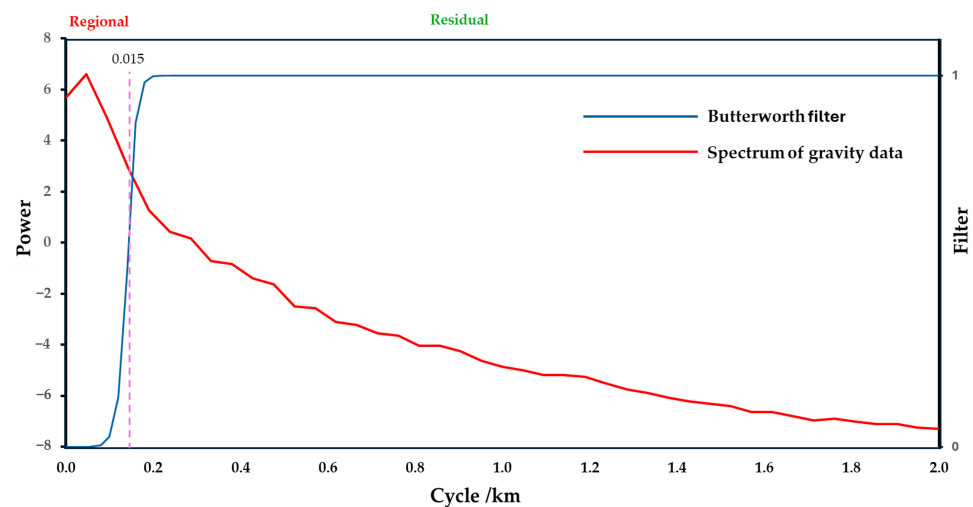


**Figure 4.** The radially averaged power spectrum of the gravity data. The red line represents the spectrum signal, while the blue line illustrates the design of the Butterworth filter, which has a cutoff wavenumber of 0.15 cycles/km (purple dashed line) and a filter order of 8. The high-pass filter attenuates longer wavelengths, producing residual anomalies that reveal shallow geological features of interest.

For obtaining the appropriate cutoff wavenumber, we conducted a spectral analysis on the Complete Bouguer Anomaly using the radially averaged power spectrum (RAPS), as shown in Figure 4. By analyzing the gradient of the regional signal in the power spectrum, we determined that the appropriate cutoff wavenumber should be approximately 0.15 cycle/km, which corresponds to a wavelength cutoff of approximately 6.5 km. Furthermore, through a process of trial and error in filtering, we compared the resulting residual anomalies with surface lithological distributions and structures in the study area. This iterative approach allowed us to refine the selected cutoff, ensuring that the filtered residual anomaly represents the shallow geological features of interest.

## 4.2. Three-Dimensional Geological Modeling

A 3D geological model was constructed based on prior studies and interpretations [5,8,35,36]. Geological modeling was carried out using Geomodeller [45,46]. The software adopted an interpolation algorithm based on iso-potential field theory, which allows us to construct complex geological models using various inputs of geological data. The geometry of geological formations is determined by interpolating a continuous 3D iso-potential surface of a given geological layer, using both surface and subsurface geological data such as geological contacts, formation dips, and orientations. The modeling process incorporates structural data and stratigraphic rules to produce a reliable 3D geological model. Detailed information regarding the methods of geological modeling is reported by Calcagno et al. [46] and Guillen et al. [45]. Additionally, the software allows for the creation of geophysical datasets based on the 3D geological model, which is highly useful for geophysical forward modeling and inverse modeling.

In this research, we constructed 3D geological models using a pseudo-3D reconstruction approach, which utilizes several 2D geological sections to build the 3D model. We defined six 2D geological cross-sections to create the 3D geological model (Figure 5). Due to the limited availability of data, especially at depth, geological concepts and existing geological sections and interpretations (e.g., [5,8,35,36]) were used to estimate the geometric approximation and lateral continuity of the geological body in the deeper area. In addition, the top surface was provided by SRTM30 DEM.
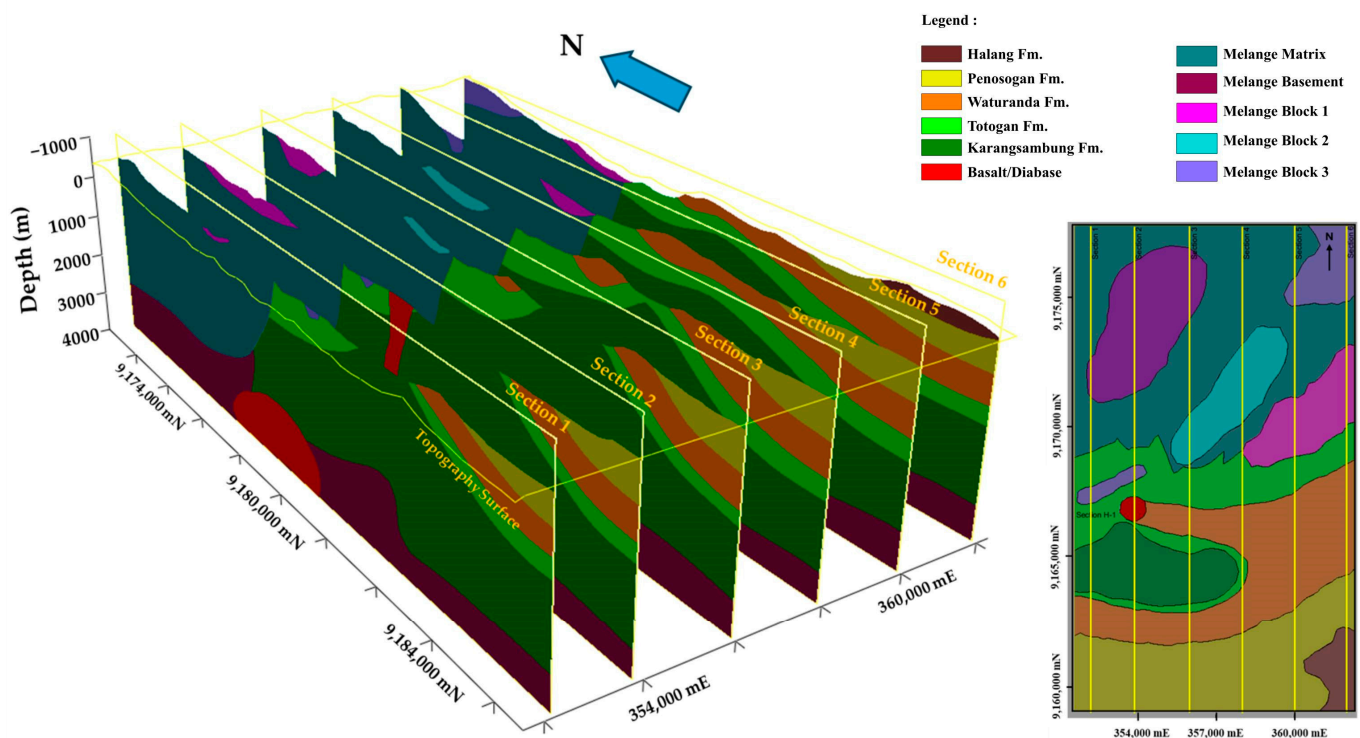


**Figure 5.** The construction of a 3D geological model utilizing six geological cross-sections based on previous studies and interpretations [5,8,35,36].

## 4.3. Forward Modeling and Building Optimal a Priori Model

In this stage, our primary objective is to develop an optimal a priori model based on the 3D geological model, which will be evaluated and refined in the subsequent inverse modeling stage. The forward modeling was developed based on the methodologies described in [47,48], and implemented within Geomodeller software (version 4.0.8). The forward modeling was performed iteratively, with several experimental variations of measured density, as shown in Table 1. For each iteration, the results were compared with the residual gravity anomaly to evaluate the gravity response of the forward model, ensuring

it matched the observed data in terms of anomaly range and minimal misfit error. This step is crucial for defining the optimized density and update the 3D model, which will then be selected as the a priori model and starting density for use in the inverse modeling.

To proceed with the modeling, the 3D geological model was discretized into a grid of voxels or cells. Each voxel was assigned a density corresponding to its lithology, allowing for the calculation of the model's gravitational response through forward modeling. The dimensions of each voxel were set to 250 m $\times$ 250 m horizontally, with a height of 50 m. The densities assigned during forward modeling were determined based on the measured densities of rock samples (Table 1). The modeling process also considers the topography as an elevation reference for gravity computation. The area above the topography was assigned a density of 2.61 g/cm$^3$, consistent with the reference density used in the computations.

### 4.4. Three-Dimensional Inverse Modeling

3D gravity inversion was carried out to optimize the fit between calculated gravity anomalies from the a priori model and observed residual anomalies, as well as to gain detailed insights into the spatial distribution of subsurface density. The general inverse problem in geophysics can be expressed using Equation (2).

$$\boldsymbol{m} = G^{-1}(\boldsymbol{d}) \tag{2}$$

In this equation, $\boldsymbol{m}$ represents the model, $\boldsymbol{d}$ denotes the data, and $G^{-1}$ is the inverse operator used to derive the model parameters $\boldsymbol{m}$ from the observed data $\boldsymbol{d}$. However, directly inverting $G^{-1}$ is often impractical because the problem may be underdetermined due to insufficient data or uncertainties present in the experimental process. The general Bayesian approach to solve the inverse problem can be expressed in Equation (3) [49].

$$P(\boldsymbol{m}) = c\rho(\boldsymbol{m})L(\boldsymbol{m}) \tag{3}$$

where $c$ is a suitable normalization constant. The posteriori probability density, $P(\boldsymbol{m})$, is calculated as the product of the a priori probability density, $\rho(\boldsymbol{m})$, and a "likelihood function", $L(\boldsymbol{m})$ This likelihood function, in basic terms, evaluates how well the observed data match the data predicted by the model **m**. In this stochastic inversion, the likelihood function is computed using Equation (4), where $\sigma^2$ denotes the variance of the data. The misfits $S(\boldsymbol{m})$ representing the difference between the calculated $g_n(\boldsymbol{m})$ and observed data $d_n$, is determined using Equation (5).

$$L(\boldsymbol{m}) = c\exp\left(\frac{-S(\boldsymbol{m})}{\sigma^2}\right) \tag{4}$$

$$S(\boldsymbol{m}) = \frac{1}{2}\sum_{n=1}^{N}(g_n(\boldsymbol{m}) - d_n)^2 \tag{5}$$

The 3D stochastic inverse modeling was carried out using Geomodeller software (version 4.0.8), employing a Monte Carlo sampling approach to explore possible solutions. This method allows for the incorporation of multiple geological constraints during the inversion process. These constraints are necessary to mitigate the non-uniqueness of gravity inversion results, especially in the absence of borehole data. The inversion strategy and procedures described by Guillen et al. [45] are summarized below, and the simplified workflow of the inversion process is illustrated in Figure 6.
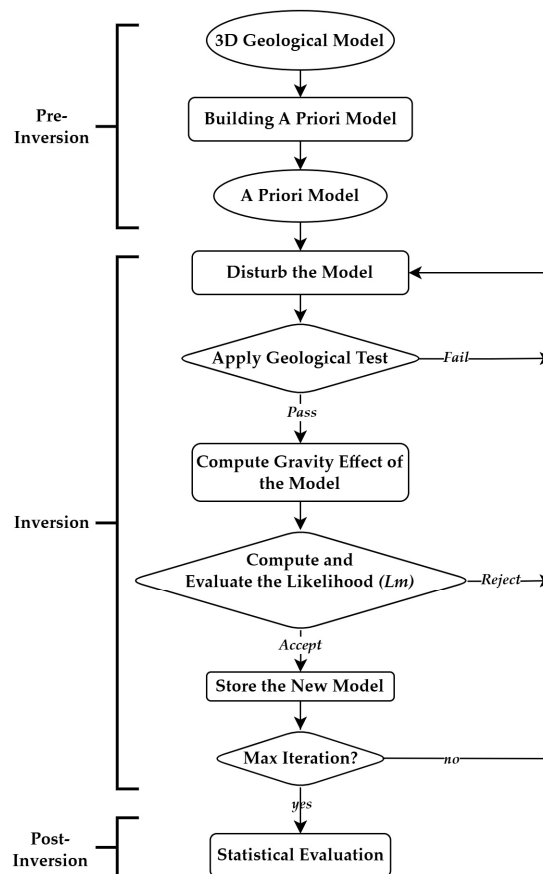
**Figure 6.** A generalized flowchart of the stochastic inversion process for gravity data. This approach allows for the integration of various geological constraints during model perturbation to ensure that the inverted model remains geologically reasonable.

1.  Development of the a priori model.

    This early step has been discussed in Section 4.3.

2.  Discretization.

    The a priori model must be discretized into a sum of regular cubic cells, referred to as voxels, to facilitate computation during the inversion. The same cell size of 250 m × 250 m horizontally and a height of 50 m, which was established in the forward modeling, is used in the inversion process.

3.  Parameterization.

    At the start of the inversion, the optimized densities from Table 1 are used as the initial density inputs for the a priori model. Each lithology in the model has specific constraints to limit density changes during inversion, reflecting the heterogeneity of the formations in the study area. Additionally, density variations from measured rock samples, along with experimental data on rock type densities from [40,50], were considered when establishing these constraints, as recommended by Bosch et al. [51]. The density constraints for each formation used in the inversion are presented in Table 2. The constraint is applied using a normal distribution characterized by a mean value and a standard deviation.

**Table 2.** The user-defined parameters for constraining the stochastic inversion. Petrophysical and lithological constraints are applied to ensure geologically reasonable results.

| No | Lithology | Density Constrain | | Shape Ratio | | Volume Ratio | | Commonality | | Classification |
|----|-----------|------|-----|------|-----|------|-----|-------|-------|----------------|
| | | Mean | Std | Mean | Std | Mean | Std | Scale | Shape | |
| 1 | Luk-Ulo Melange Complex | | | | | | | | | |
| | a. Melange Matrix | 2.36 | 0.1 | 1 | 0.05 | 1 | 0.05 | 0.3 | 1 | Loose |
| | b. Melange Block 1 | 2.79 | 0.05 | 1 | 0.05 | 1 | 0.05 | 0.3 | 1 | Moderate |
| | c. Melange Block 2 | 2.65 | 0.05 | 1 | 0.05 | 1 | 0.05 | 0.3 | 1 | Moderate |
| | d. Melange Block 3 | 2.66 | 0.05 | 1 | 0.05 | 1 | 0.05 | 0.3 | 1 | Moderate |
| | e. Basement | 2.85 | 0.1 | 1 | 0.07 | 1 | 0.07 | 0.5 | 1 | Loose |
| 2 | Karangsambung Fm. | 2.37 | 0.1 | 1 | 0.03 | 1 | 0.03 | 0.2 | 1 | Moderate |
| 3 | Totogan Fm. | 2.48 | 0.1 | 1 | 0.03 | 1 | 0.03 | 0.2 | 1 | Moderate |
| 4 | Diabase | 2.78 | 0.05 | 1 | 0.05 | 1 | 0.05 | 0.3 | 1 | Moderate |
| 5 | Waturanda Fm. | 2.63 | 0.07 | 1 | 0.05 | 1 | 0.05 | 0.2 | 1 | Moderate |
| 6 | Panasogan Fm. | 2.48 | 0.05 | 1 | 0.03 | 1 | 0.03 | 0.2 | 1 | Moderate |
| 7 | Halang Fm. | 2.62 | 0.05 | 1 | 0.02 | 1 | 0.02 | 0.2 | 1 | Strict |

4. Sampling and disturbing the model.

5. During each iteration, the current model is perturbed by modifying either the petrophysical properties individually or both the petrophysical properties and the lithological boundaries. In this inversion, the probability of lithological change at the formation boundary is set at 50%. The sampling method follows the approach described in [52].

6. Application of the geological test.

If lithological changes occur in the previous step, a geological test must be conducted to ensure that the perturbed model maintains geologically reasonable results. In this case, the geological test was adjusted to follow user-defined geological constraints, which are controlled by parameters such as shape ratio, volume ratio, and commonality, all integrated into the software. The shape and volume ratio parameters, which regulate the extent of formation changes in terms of shape and volume relative to the reference model, are controlled using a normal probability density function. Meanwhile, the commonality parameter, which limits formation changes by ensuring overlap with the reference model, is constrained by a Weibull probability density function. Specific settings for these parameters are provided in Table 2. The classification column in Table 2 defines the level of constraint applied to the inversion parameters, categorized as strict, moderate, or loose. A 'Strict' setting ensures that the inversion produces minimal deviations from the reference model. A 'Moderate' setting permits a broader range of adjustments, while still adhering to the general framework of the reference model. A 'Loose' setting allows for greater flexibility, enabling more substantial changes with fewer restrictions. These inversion constraints were determined based on the confidence levels of the input data, including specific location, distribution, and interpretation from previous studies [5,8,35,36]. Additionally, surface geology was not fixed, allowing changes in both subsurface and surface lithologies.

7. Computation of the gravity effect of the disturbed model.

8. Computation and evaluation of the likelihood of the perturbed model $L(m_{pert})$.

The likelihood of perturbed model $L(m_{pert})$ can be calculated using Equation (4). $S(m_{pert})$ represents the misfit between the perturbed and observed gravity data. The perturbed model ($m_{pert}$) is evaluated against the currently accepted model ($m_{curr}$) using Metropolis sampling criteria [53]:

- If $L(m_{pert}) > L(m_{curr})$, accept $m_{pert}$
- If $L(m_{pert}) <= L(m_{curr})$, accept $m_{pert}$ with random sampling and a probability $L(m_{pert})/L(m_{curr})$
- If ($m_{pert}$) is accepted, then store the perturbed model, set $m_{curr} = m_{pert}$. But, if $m_{pert}$ is rejected, $m_{curr}$ is not modified.

9.    Return to step 4, and repeat the process.

Before reaching the maximum number of iterations, the inversion returns to step 4 and continues to iterate around this loop until the maximum iteration is achieved. In this inversion, the iterations are set to a maximum of 50 million, a large number necessary to ensure that each cell in the model is visited multiple times during the inversion. At the end of the iterations, the statistical evaluation of the inversion regarding the changes in the petrophysical properties and lithologies after inversion is calculated to obtain the inverted density model and the most probable subsurface model.

## 5. Results

### 5.1. Residual Gravity Anomaly

The residual gravity anomaly, derived by applying a high-pass filter to the complete Bouguer Anomaly (CBA), serves as a crucial tool for validating and refining the geological model prior to initiating the inversion process, as outlined in Section 4.3. Figure 7 depicts the residual gravity anomaly, which ranges from −6.72 to 7.18 mGal, highlighting variations in subsurface density structures across the region. In the southern region, low gravity anomalies are associated with the Karangsambung and Totogan formations, both of which are characterized by relatively low-density materials, as indicated in Table 1. At Mt. Parang, the distribution of diabase correlates with the presence of high-gravity anomalies. Diabase, being a dense igneous rock, contributes to the elevated gravity readings in this area, consistent with the presence of significant volcanic intrusions.
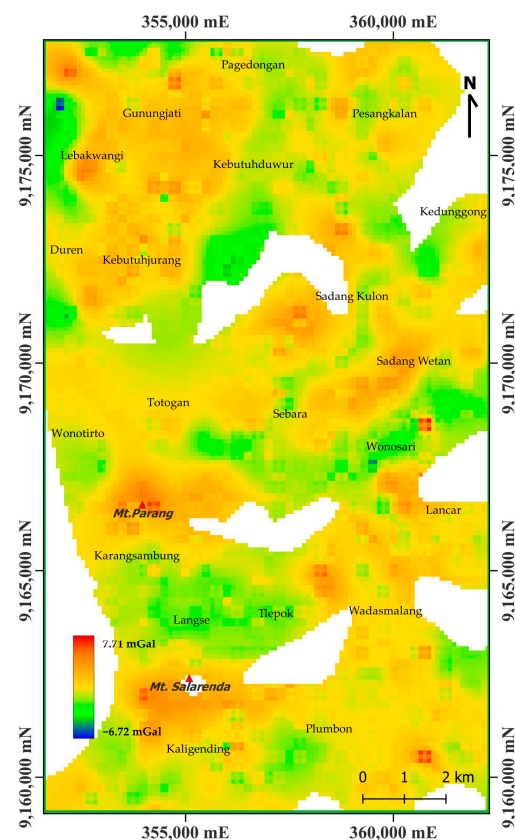


**Figure 7.** Residual gravity anomalies (−6.72 to 7.18 mGal) derived from a high-pass filtered Complete Bouguer Anomaly (CBA). Low anomalies in the south correspond to low-density Karangsambung and Totogan formations, while high anomalies at Mt. Parang indicate dense diabase intrusions. In the north, negative anomalies reflect the matrix of the Luk-Ulo Melange Complex, and positive anomalies highlight high-density rocks like schist, gabbro, and serpentinite. The red triangle denotes the location of the mountains.

In the northern region, local variations in gravity anomalies are more pronounced. Low negative anomalies are indicative of the matrix distribution within the Luk-Ulo Melange Complex (LMC), which is a tectonic mixture of diverse rock types with varying densities. This region contains lower-density rocks such as melange matrix, leading to the observed negative anomalies. Conversely, strong positive anomalies in this area correspond to the presence of high-density rocks, including schist, phyllite, gabbro, and serpentinite [5,35].

### 5.2. A Piori Model

In the northern area, constructing the model is challenging due to the unclear geological contacts, especially regarding the distribution of melange blocks within the Luk-Ulo Melange Complex (LMC). To address this, gravity anomalies were used to estimate the geometry and lateral continuity of the geological bodies. Additionally, optimized densities for melange blocks were introduced based on selected rock samples such as gabbro, serpentinite, and phyllite/schist, which are commonly found in this area [5,34,35]. In the present model, the Luk-Ulo Melange Complex (LMC) was modeled as isolated bodies of high-density rocks with various lithologies, embedded within a low-density scaly clay matrix. Table 1 shows the optimized densities used in the forward a priori modeling. At greater depths, the basement is introduced as the oldest stratigraphic layer, characterized by a high density.

At Mt. Parang, while diabase outcrops are abundant, the vertical continuity of the diabase remains uncertain due to the absence of borehole data. Consequently, two different models were initially proposed: an intrusive model and a block-in-matrix model, to explain the positive anomalies in the area. Both models were then subjected to 2D forward modeling using the optimized densities listed in Table 1 and their results are evaluated and presented in Figure 8. The results indicate that the intrusive model shows less inconsistency with the observed gravity data in terms of anomaly range and misfit errors compared to the block-in-matrix model. Moreover, the intrusive body model corresponds with the distribution of high-gravity anomalies in the Complete Bouguer Anomaly map (Figure 3b), located slightly north of Mt. Parang. Based on these findings, the intrusive model was chosen and implemented in constructing the final a priori model.
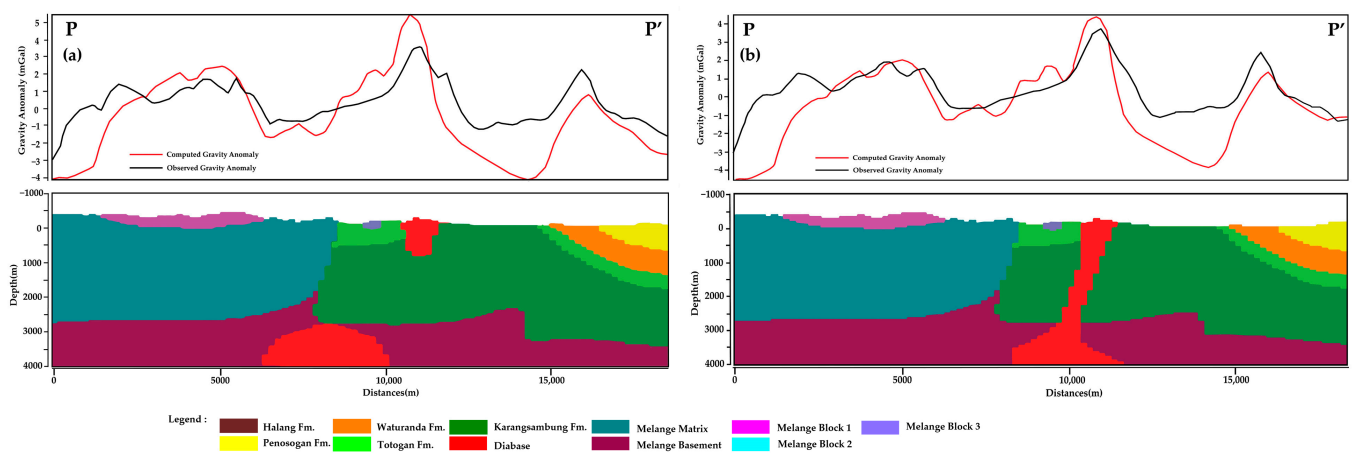


**Figure 8.** The results of the iterative trial-and-error process for 2D forward modeling along the P–P′ profile for two proposed database models: the block-in-matrix model (**a**) and the intrusive model (**b**). The red line represents the calculated anomaly, while the black line shows the observed anomaly.

In addition, the Tertiary sedimentary rocks, predominantly distributed in the southern areas, were modeled as layered rock formations with two opposing dip directions, resulting in the formation of an anticline structure. Near the surface, the horizons and thicknesses of each formation in the model were varied according to the geological cross-sections from

Asikin et al. [35] and further refined through the fitting and comparison process during the construction of the final a priori model. The final 3D a priori model is presented in Figure 9.
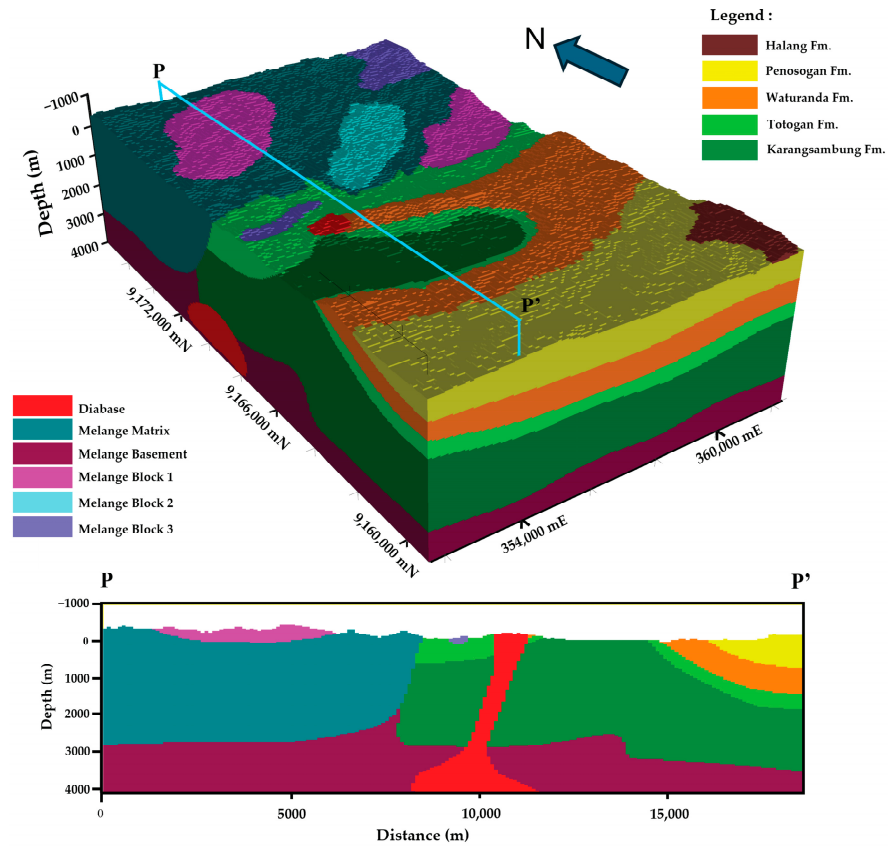


**Figure 9.** Three-dimensional a priori model of the study area, showing the P–P' (N–S cross-section) profile with highlighted dike intrusions beneath Mt. Parang. The model is discretized into cubic cells, enabling the forward calculation of gravity responses based on the assigned density contrasts for each cell.

*5.3. Inverted Model*

The performance of the inversion can be evaluated based on its misfit, which represents the inconsistency error between the observed data and the proposed or inverted model. Figure 10 illustrates the comparison of two misfits: the misfit between the observed gravity data and both the forward a priori model and the forward inverted model, accompanied by their respective histograms. Given the presence of blank areas within the observed anomaly, the computation of likelihood and misfit values during the inversion process is limited to regions with valid data. The results indicate that the forward a priori model achieves a Root Mean Squared Error (RMSE) of 2.71 mGal when compared to the observed gravity data (Figure 10a).
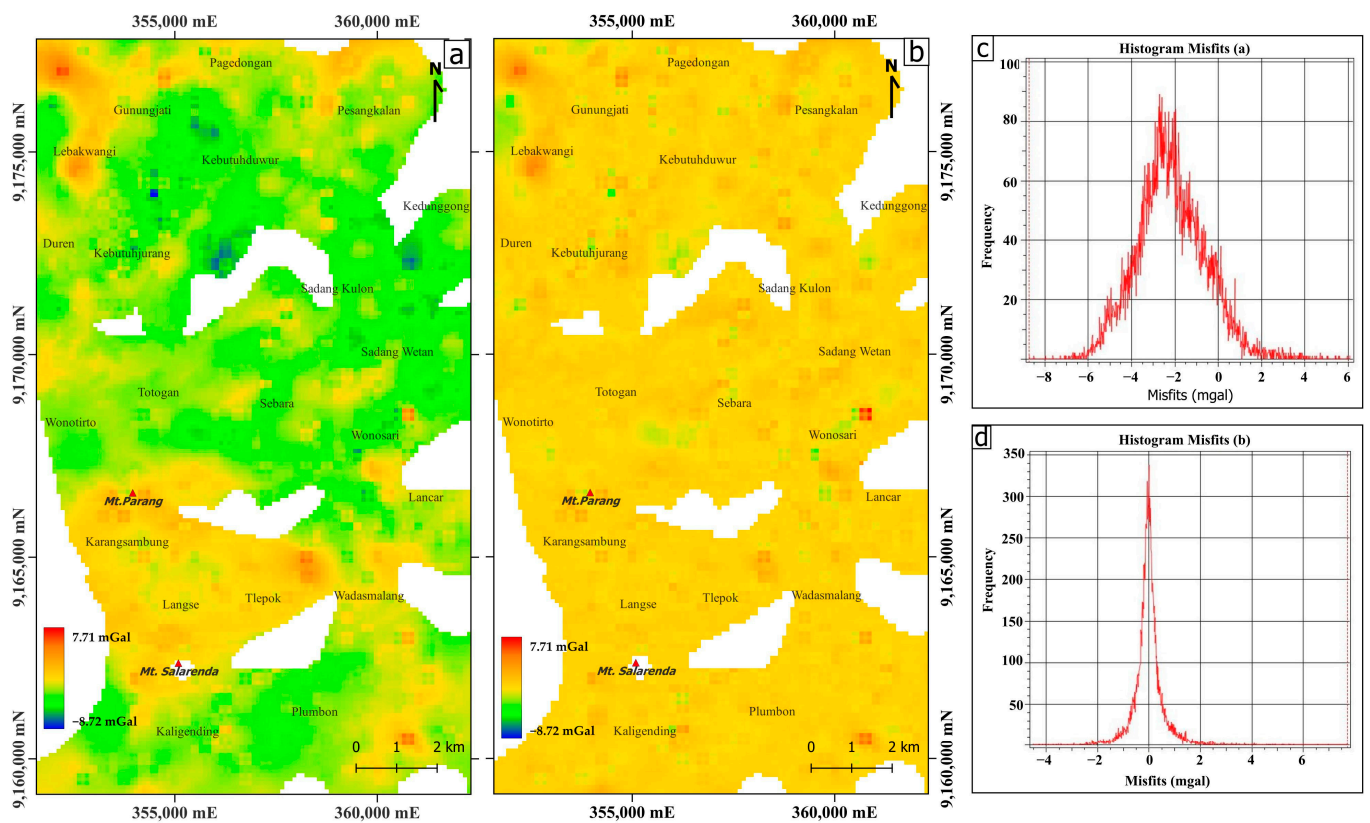
**Figure 10.** The misfit distribution between observed gravity and the forward a priori model (**a**) and between observed gravity and the forward inverted model (**b**). Reddish areas indicate regions with high positive misfit, while bluish areas indicate regions with high negative misfit. The histograms show a decrease in average misfit values from −2.18 mGal in the initial forward model (**c**) to −0.0068 mGal in the inverted model (**d**), demonstrating the effectiveness of the inversion process. The red triangle denotes the location of the mountains.

The inversion performance, shown in Figure 11, demonstrates a decrease in misfit as iterations increase, ultimately achieving a final RMSE of 0.55 mGal after 50 million iterations. This suggests that the inversion process successfully minimized the misfit by approximately 80% relative to the a priori model. This result is further supported by the reduction in the average misfit, as shown in the histogram, from −2.18 mGal before inversion to −0.0068 mGal afterward. Although additional inversion iterations were attempted to further reduce the misfit, these efforts increased processing time and produced results increasingly inconsistent with geological concepts. This discrepancy arises because the misfit error is exceptionally high in areas with extreme gravity anomalies, making it challenging to achieve low misfits in those regions during the inversion process.

Table 1 provides a detailed report on the changes in density and volume following the inversion. The average densities of Melange Block 1, Melange Block 2, and Melange Block 3 increased by 0.01 g/cm$^3$, 0.05 g/cm$^3$, and 0.03 g/cm$^3$, respectively, while their volumes decreased by 0.24%, 0.04%, and 0.02%, respectively. In contrast, the melange matrix showed an increase in both average density (by 0.06 g/cm$^3$) and volume (by 2.3%). These changes suggest that the matrix has expanded and the blocks have shrunk, indicating a higher proportion of matrix relative to blocks within the Luk Ulo Melange Complex (LMC). Additionally, the inversion process resulted in a slight decrease in both the average density (by 0.01 g/cm$^3$) and volume (by 0.14%) of the diabase. The minimal changes in these parameters suggest that the geometry of the diabase closely matches the a priori model, confirming its stability during the inversion.
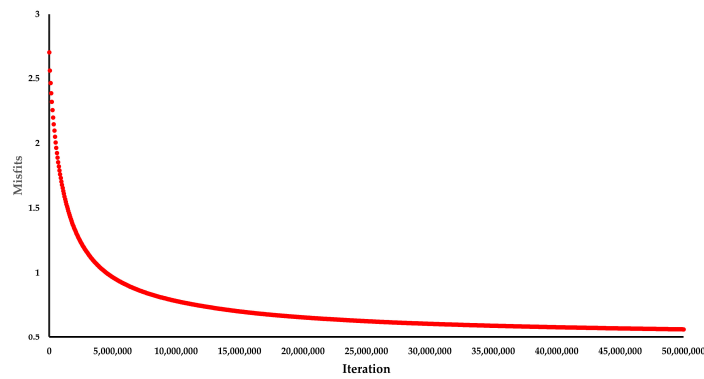
**Figure 11.** A graph showing the performance of the inversion process is presented, with the misfit plotted against the number of iterations. It can be inferred that the misfit decreases as the number of iterations increases, indicating the convergence of the inversion process.

The comparison between the top surfaces of the a priori and inverted models is shown in Figure 12. The results indicate that surface interfaces did not change significantly from the a priori model, with notable changes observed only in the Mt. Parang and Sadang Wetan areas. In Sadang Wetan, the surface distribution and volume of isolated Melange Block 1 became smaller and thinner compared to the a priori model. This result suggests that the proportion of the melange matrix, indicated by a low density ($2.42 \pm 0.053$ g/cm$^3$), within the melange is higher than the proportion of blocks, indicated by a high density ($2.69$–$2.80$ g/cm$^3$).
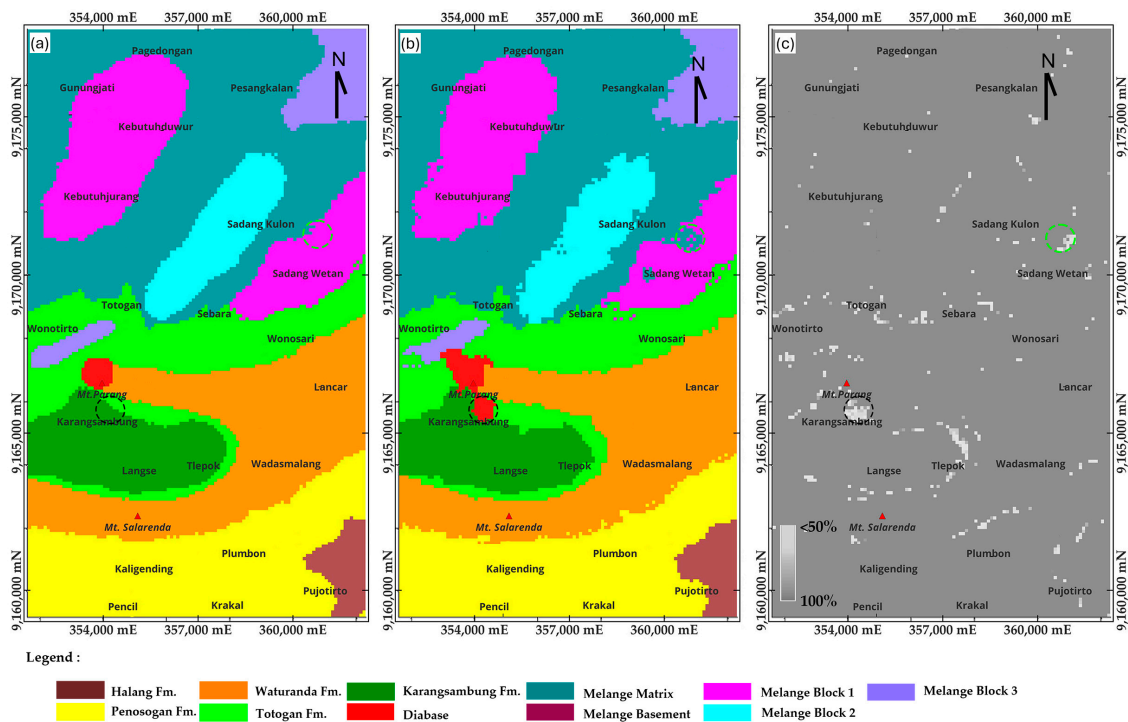


**Figure 12.** The top surface of the 3D a priori model represents the lithological distribution in Karangsambung (**a**). The top surface of the inverted model shows changes in the lithological interface after inversion (**b**). Notable changes on the surface of the inverted model, compared to the a priori model, are particularly evident in Sadang Wetan and Mt. Parang, highlighted by green and black dashed circles, respectively. The percentage probability values in (**c**) indicate the uncertainty and confidence levels of the perturbed model after inversion, with low and high probability values represented by white and gray, respectively. The red triangle denotes the location of the mountains.

In Mt. Parang, the inverted model reveals the presence of a small diabase distribution, as indicated by the black dashed circle in Figure 12. This finding suggests that the small, separated diabase distribution does not extend downward, unlike the main diabase intrusion, raising the possibility of a diabase block within the melange deposits. However, this separated distribution is associated with a low probability value (<60%) in Figure 12c, indicating a high level of uncertainty regarding the existence of the diabase block. Further analysis of the inverted model along profile P-P' suggests that this small distribution of diabase could still be interpreted as a lateral extension or continuity of the main diabase body near the surface (Figure 13). At a depth of approximately 3 km below Mt. Parang, the intrusion widens and becomes larger, indicating the possible presence of a magma source. The magma has likely cooled and formed a high-density igneous rock, which corresponds to the strong positive anomaly observed in the Complete Bouguer Anomaly (CBA) near Mt. Parang, Wonotirto, and Totogan, likely representing a high-density rock body at a deeper source (Figure 13b).
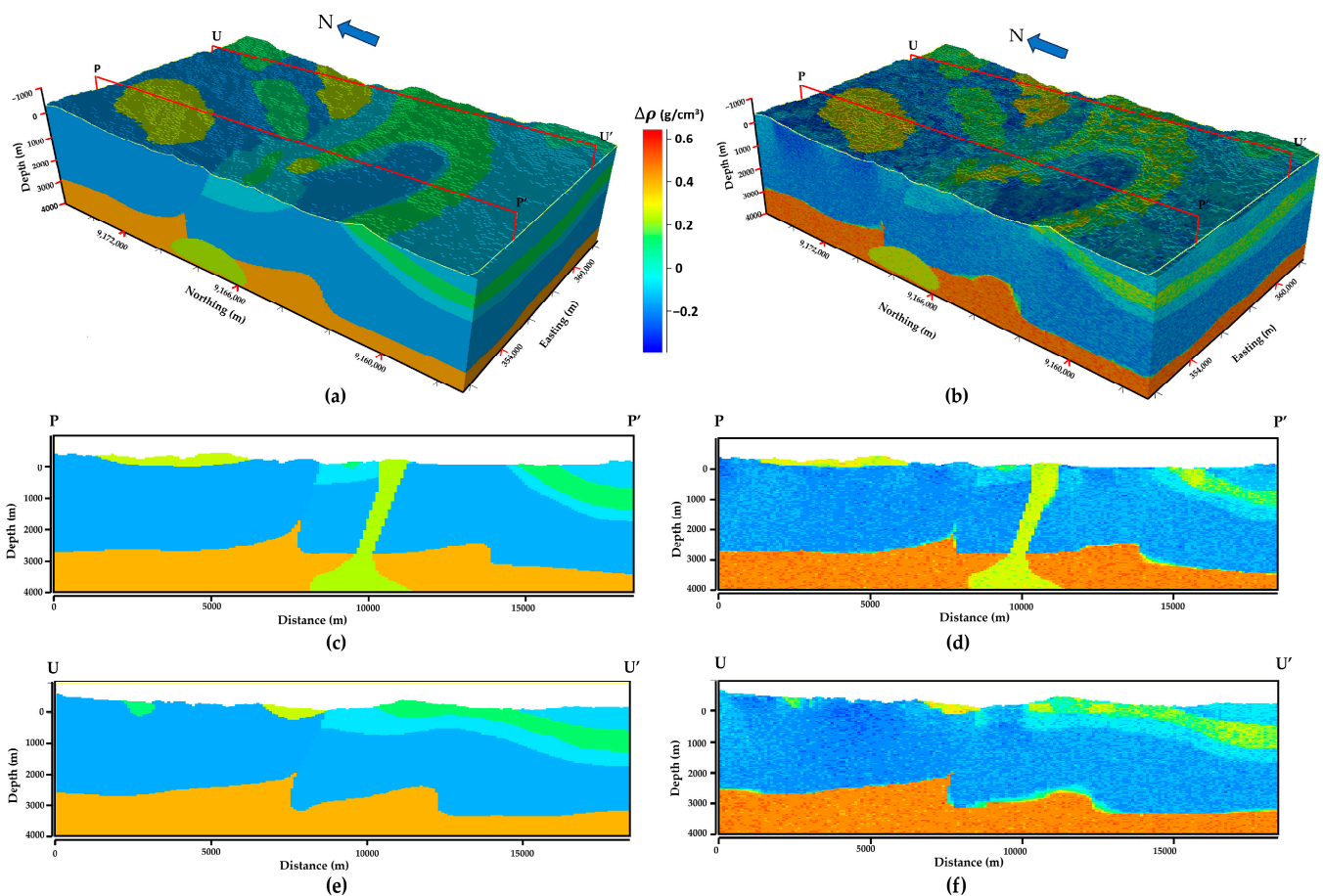


**Figure 13.** The 3D discrete a priori model serves as a starting model in the inversion (**a**). The inverted model, which reflects the new density distribution in the 3D model, is shown in (**b**). The colors indicate the contrast densities assigned to each cell, with the red-to-blue color bar representing high to low contrast densities. A background density of 2.61 g/cm$^3$ was used in the modeling. Comparisons between the a priori model and the inverted model along the P–P' section are shown in (**c**,**d**), and along the U–U' section in (**e**,**f**). Along P–P', a decrease in the volume of the Waturanda Formation, compared to the a priori model, is highlighted by the red dashed line. Detailed changes in each lithology are presented in Table 1.

In the southern area, where the lithology is dominated by Tertiary sedimentary rocks, the density and volume of the Karangsambung Formation increased by 0.05 g/cm$^3$ and 0.89%, respectively. Similarly, the average density and volume of the Totogan Formation

increased by 0.05 g/cm$^3$ and 0.19%, respectively. The average densities of the Tertiary sedimentary rocks, including the Waturanda, Penosogan, and Halang formations, generally decreased. However, changes in volume among these sedimentary rocks varied, with the Waturanda Formation experiencing the most significant decrease at 0.62%. The variation in volume and thickness changes in each sedimentary rock compared to the a priori model is depicted in Figure 13. It can be inferred that the thickness of the Waturanda Formation decreases as the thickness and volume of the Penosogan, Totogan, and Karangsambung formations increase (Figure 13d).

## 6. Discussions

The origin of diabase in Mt. Parang has been discussed in previous studies [8,18,37]. In this study, we present our interpretation based on 3D gravity data modeling. The results from both forward and inverse modeling at Mt. Parang suggest that the origin of the diabase is a dike intrusion, possibly related to volcanic activity (Figure 13). According to the inverted model, the intrusion cuts through the Karangsambung and Totogan formations, with an average density of the diabase intrusion of 2.77 ± 0.051 g/cm$^3$. The proposed intrusion model exhibits only minimal changes in volume and density during the inversion process (Table 1). Crucially, the inversion process, which required 50 million iterations, successfully preserved the geometry of the intrusion. The only significant change in the model is the appearance of a small, newly separated body of diabase at the surface. However, this new distribution has a low probability value (0.50%), indicating a high degree of uncertainty in the model. Overall, the inversion results align with previous geological studies [5,8,35] and geophysical approaches [15,17,21,54]. However, there is a discrepancy with the findings of Handayani et al. [18] regarding near-surface structures that showed the discontinuity of diabase at depth, likely due to the limited coverage and the different geophysical methods employed, such as the use of electrical resistivity primarily for near-surface investigations.

In addition to the diabase intrusion, the inverted model indicates the presence of a solidified magma reservoir at a depth greater than 3.5 km, located slightly north of Mt. Parang. This feature is highlighted in Figure 14, where the model shows the intrusion body and the potential solidified magma reservoir. The presence of this high-density solidified magma reservoir is also suggested by a strong positive anomaly in the central region of the Complete Bouguer Anomaly map (Figure 3b). This solidified magma reservoir may be associated with the genesis of the Tertiary Dakah Volcano, as mentioned by Setiawan et al. [8], based on geological field surveys and petrological analyses. The research suggests that the shallow diabase intrusion is one of the products of volcanic activity with island arc tholeiite affinities. Based on K-Ar dating of diabase in Parang conducted by Soeria-Atmadja et al. [9], Setiawan et al. [8] estimate that the Dakah Volcano may have been active during the Late Eocene to Early Oligocene. However, the depth of the Dakah solidified magma reservoir remains uncertain due to the lack of borehole data or seismic activity records from this ancient volcanic event. To provide context, we compared our results with the depths of magma reservoirs in modern volcanoes, such as Mt. Merapi and Mt. Agung, which have been estimated using seismic tomography imaging. The shallow magma reservoirs in these volcanoes are estimated to be located between approximately 1 and 5 km from the summit [55,56]. Our comparison suggests that the depth of the Dakah solidified magma reservoirs is shallower than those of modern volcanoes. This could be explained by tectonic activity related to regional uplift that occurred during the Oligocene–Early Miocene period (35–20 Ma), as described by Sribudiyani et al. [31].
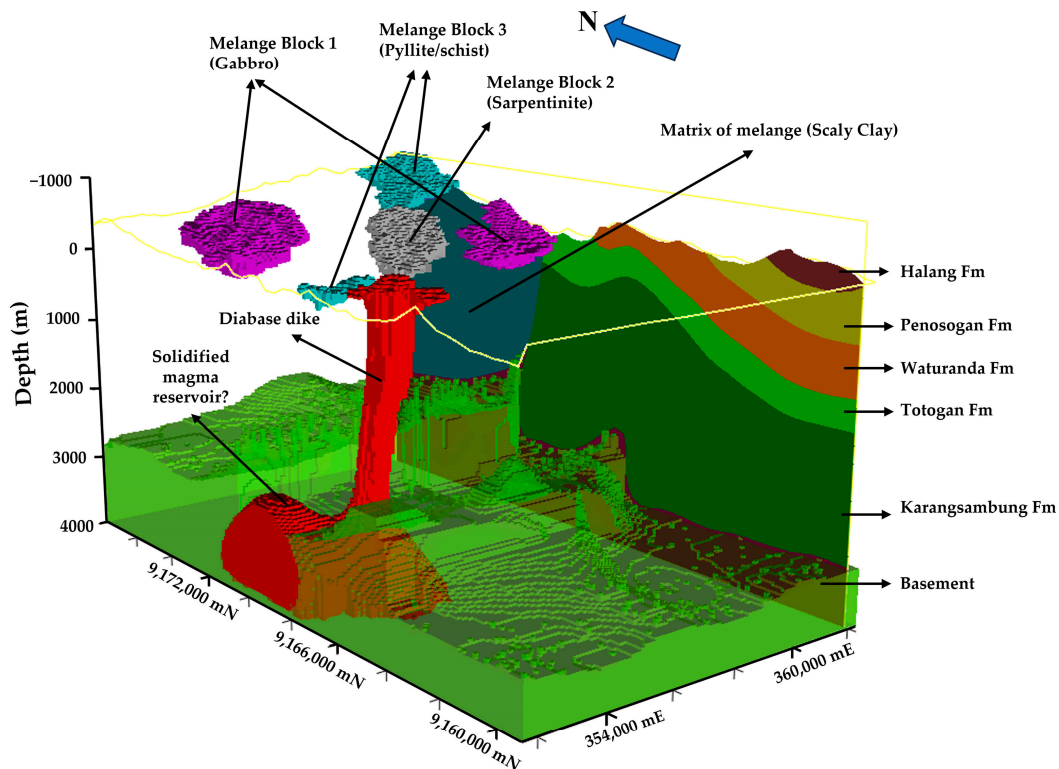
**Figure 14.** The most probable result of the stochastic inversion suggests the presence of a diabase intrusion beneath Mt. Parang. This dike intrusion cuts through both the Karangsambung and Totogan formations, eventually being exposed at the surface. At a depth of approximately 3 km beneath Wonotirto and Totogan, a larger rock body appears, indicating the potential presence of a solidified magma reservoir. This solidified magma reservoir may be linked to the genesis of the Dakah volcanism during the Late Eocene to Early Oligocene [7,8]. Additionally, the modeling successfully identifies the block-matrix structure of the Luk-Ulo Melange Complex (LMC) in the northern area. The blocks are characterized by high-density rock (2.69–2.80 g/cm$^3$) floating within the low-density scaly clay matrix (2.42 ± 0.053 g/cm$^3$). The yellow line denotes the surface topography.

According to our modeling results, the Luk Ulo Melange Complex can be simplified into two zones based on depth: the shallow zone and the deeper zone. In the shallow zone, the inverted model indicates that the area is characterized by high-density isolated blocks embedded within low-density matrices. The high-density rocks are likely serpentinite (2.70 ± 0.057 g/cm$^3$), gabbro (2.80 ± 0.060 g/cm$^3$), and phyllite (2.69 ± 0.057 g/cm$^3$), while the low-density matrix is probably composed of scaly clays (2.42 ± 0.053 g/cm$^3$). The block-matrix structure of the Luk Ulo Melange Complex is illustrated in Figure 14. This model is consistent with previous surface geological studies by Asikin [5] and Suparka [34], which describe the characteristics of the Luk Ulo Melange Complex. The deeper zone, on the other hand, is characterized by high-density crystalline rocks, most likely igneous in origin. Based on the inverted model, the density of the basement is estimated to be 2.85 ± 0.050 g/cm$^3$, comparable to the measured densities of gabbro (2.75–2.90 g/cm$^3$) in the study area. Unfortunately, due to the lack of borehole data, the measured density of the basement rock is not available, precluding further analysis.

We acknowledge that potential field modeling is subject to various uncertainties, including assumptions and the subjectivity of forward modeling due to limited data distribution, especially at depth. First, the contacts between lithologies in deeper areas are subjectively estimated based on previous geological and geophysical studies in the region, particularly regarding the melange basement. The geological contacts in the model are estimated based on cross-sections provided by Asikin et al. [35]. Second, the inversion results depend on the starting model and the inversion parameters that control model

perturbation during the inversion process. Therefore, we carefully checked every inversion parameter to ensure consistency with geological constraints based on the available data and evaluated each result statistically to minimize model ambiguity.

## 7. Conclusions

The study highlights the integration of 3D geological modeling and gravity surveys to infer the subsurface structure in Karangsambung. The newly expanded gravity data coverage, particularly in Mt. Parang and the Luk Ulo Melange Complex (LMC), provides fresh insights through 3D gravity modeling. The inverted model shows that the diabase outcrops in Mt. Parang are an intrusion in origin which may be related to the genesis of Dakah volcanism. The modeling results also estimate the depth of the shallow solidified magma reservoir of Dakah volcanic unit to be approximately 3 to 4 km beneath Mt. Parang. Additionally, the 3D gravity model reveals that the subsurface structure beneath the LMC in the northern area can be divided into two zones based on depth. The shallow zone is characterized by a mix of low- to high-density rocks, indicating matrix-block interactions within the melange deposit. In contrast, the deeper zone is dominated by high-density crystalline rock, most likely igneous and compositionally similar to gabbro. Recognizing that potential field modeling is subject to various uncertainties, we meticulously checked each inversion parameter against geological constraints and evaluated the results in the context of previous studies to minimize model ambiguity.

## References

1. Hall, R. Late Jurassic–Cenozoic Reconstructions of the Indonesian Region and the Indian Ocean. *Tectonophysics* **2012**, *570–571*, 1–41. [CrossRef]
2. Hamilton, W. *Tectonics of the Indonesian Region*; U.S. Geological Survey Professional Paper; US Government Printing Office: Washington, DC, USA, 1979; Volume 1078. [CrossRef]
3. Wakita, K. Cretaceous Accretionary–Collision Complexes in Central Indonesia. *J. Asian Earth Sci.* **2000**, *18*, 739–749. [CrossRef]
4. Festa, A.; Pini, G.A.; Dilek, Y.; Codegone, G. Mélanges and Mélange-Forming Processes: A Historical Overview and New Concepts. *Int. Geol. Rev.* **2010**, *52*, 1040–1105. [CrossRef]
5. Asikin, S. *Evolusi Geologi Jawa Tengah Berdasarkan Teori Tektonik Dunia Yang Baru*; Institut Teknologi Bandung: Bandung, Indonesia, 1974; (English Abstract Is Available).
6. Wakita, K.; Miyazaki, K.; Zulkarnain, I.; Sopaheluwakan, J.; Sanyoto, P. Tectonic Implications of New Age Data for the Meratus Complex of South Kalimantan, Indonesia. *Isl. Arc* **1998**, *7*, 202–222. [CrossRef]
7. Yuwono, Y.S. The Occurrence of Submarine Arc-Volcanism in the Accretionary Complex of The Luk Ulo Area, Central Java. *Bull. Geol.* **1997**, *27*, 15–26.
8. Setiawan, N.I.; Yuwono, Y.S.; Sucipta, I.G.B.E. The Genesis of Tertiary "Dakah Volcanic" in Karangsambung, Kebumen, Central Java. *Maj. Geol. Indones.* **2011**, *26*, 29–44.
9. Soeria-Atmadja, R.; Maury, R.C.; Bellon, H.; Pringgoprawiro, H.; Polve, M.; Priadi, B. Tertiary Magmatic Belts in Java. *J. Southeast Asian Earth Sci.* **1994**, *9*, 13–27. [CrossRef]

10.  Kapid, R.; Harsolumakso, A.H. Studi Nannoplakton pada Formasi Karangsambung Dan Totogan di Daerah Luk-Ulo, Kebumen Jawa Tengah. *Bull. Geol.* **1996**, *26*, 13–43. (English Abstract Is Available)
11.  Hayward, N.; Calvert, A.J.; Yuan, H.; Gessner, K.; Doublier, M.P. Subsurface Distribution of Granites and Greenstones in the Paleoarchean East Pilbara Terrane from 3-D Gravity Inversion. *Precambrian Res.* **2024**, *405*, 107351. [CrossRef]
12.  Dufréchou, G.; Harris, L.B.; Corriveau, L.; Antonoff, V. Gravity Evidence for a Mafic Intrusion beneath a Mineralized Zone in the Bondy Gneiss Complex, Grenville Province, Quebec—Exploration Implications. *J. Appl. Geophys.* **2011**, *75*, 62–76. [CrossRef]
13.  Nigussie, W.; Alemu, A.; Mickus, K.; Muluneh, A.A. Structure of the Upper Crust at the Axis Segmentation Stage of Rift Evolution as Revealed by Gravity Data: Case Study of the Gedemsa Magmatic Segment, Main Ethiopian Rift. *J. Afr. Earth Sci.* **2022**, *190*, 104523. [CrossRef]
14.  Haberland, C.; Bohm, M.; Asch, G. Accretionary Nature of the Crust of Central and East Java (Indonesia) Revealed by Local Earthquake Travel-Time Tomography. *J. Asian Earth Sci.* **2014**, *96*, 287–295. [CrossRef]
15.  Kamtono. *Penafsiran Penampang Gaya Berat Dua Dimensi Dan Implikasinya Terhadap Kedudukan Blok-Blok Melange Luh Ulo, Karangsambung, Jawa Tengah*; Institut Teknologi Bandung: Bandung, Indonesia, 1995; (English Abstract Is Available)
16.  Laesanpura, A.; Dahrin, D.; Sugianto, A. AMT and Gravity across praTertiary Rock Complex of Kebumen, Central Java, Indonesia. In Proceedings of the AIP Conference Proceedings, Bandung, West Java, Indonesia, 21–24 February 2017; Volume 1861, p. 030029.
17.  Santoso, D.; Suparka, E. Penafsiran Gaya Berat, Magnetik Dan Geologi Kompleks Melange Luh-Ulo, Jawa Tengah. *J. Teknol. Miner.* **1994**, *1*, 19–27.
18.  Handayani, L.; Arisbaya, I.; Mukti, M.M.; Sudrajat, Y. Determining the Origin of Volcanic Rocks in the Mélange Complex of Karangsambung Based on the Electrical Resistivity Imaging. *Isl. Arc* **2021**, *30*, e12377. [CrossRef]
19.  Cole, J.; Webb, S.J.; Finn, C.A. Gravity Models of the Bushveld Complex—Have We Come Full Circle? *J. Afr. Earth Sci.* **2014**, *92*, 97–118. [CrossRef]
20.  Barretto, J.A.L.; Dimalanta, C.B.; Yumul, G.P. Gravity Variations along the Southeast Bohol Ophiolite Complex (SEBOC), Central Philippines: Implications on Ophiolite Emplacement. *Isl. Arc* **2000**, *9*, 575–583. [CrossRef]
21.  Ahmady, F.N.; Santoso, D. Preliminary Gravity Study of Pre-Tertiary and Tertiary Rock in Northern Kebumen, Central Java, Indonesia. *IOP Conf. Ser. Earth Environ. Sci.* **2019**, *318*, 12007. [CrossRef]
22.  Beattie, D. *Gravity Modeling of a Mafic-Ultramafic Association Darvel Bay, Sabah, Northern Borneo*; Dalhousie University: Halifax, NS, Canada, 1986.
23.  Guglielmetti, L.; Comina, C.; Abdelfettah, Y.; Schill, E.; Mandrone, G. Integration of 3D Geological Modeling and Gravity Surveys for Geothermal Prospection in an Alpine Region. *Tectonophysics* **2013**, *608*, 1025–1036. [CrossRef]
24.  Amir, H.; Bijaksana, S.; Dahrin, D.; Nugraha, A.D.; Arisbaya, I.; Pratama, A.; Suryanata, P.B. Subsurface Structure of Sumani Segment in the Great Sumatran Fault Inferred from Magnetic and Gravity Modeling. *Tectonophysics* **2021**, *821*, 229149. [CrossRef]
25.  Dahrin, D.; Amir, H.; Suryanata, P.B.; Bijaksana, S.; Fajar, S.J.; Ibrahim, K.; Harlianti, U.; Arisbaya, I.; Pebrian, M.Q.; Rahman, A.A.; et al. Subsurface Structures of Sianok Segment in the GSF (Great Sumatran Fault) Inferred from Magnetic and Gravity Modeling. *Front. Earth Sci.* **2022**, *10*, 1012286. [CrossRef]
26.  Silver, E.A.; Joyodiwiryo, Y.; McCaffrey, R. Gravity Results and Emplacement Geometry of the Sulawesi Ultramafic Belt, Indonesia. *Geology* **1978**, *6*, 527–531. [CrossRef]
27.  Smyth, H.R.; Hamilton, P.J.; Hall, R.; Kinny, P.D. The Deep Crust beneath Island Arcs: Inherited Zircons Reveal a Gondwana Continental Fragment beneath East Java, Indonesia. *Earth Planet. Sci. Lett.* **2007**, *258*, 269–282. [CrossRef]
28.  Metcalfe, I. Tectonic Evolution of Sundaland. *Bull. Geol. Soc. Malays.* **2017**, *63*, 27–60. [CrossRef]
29.  Parkinson, C.D.; Miyazaki, K.; Wakita, K.; Barber, A.J.; Carswell, D.A. An Overview and Tectonic Synthesis of the Pre-Tertiary Very-High-Pressure Metamorphic and Associated Rocks of Java, Sulawesi and Kalimantan, Indonesia. *Isl. Arc* **1998**, *7*, 184–200. [CrossRef]
30.  Wakita, K.; Munasri; Bambang, W. Cretaceous Radiolarians from the Luk-Ulo Melange Complex in the Karangsambung Area, Central Java, Indonesia. *J. Southeast Asian Earth Sci.* **1994**, *9*, 29–43. [CrossRef]
31.  Sribudiyani, S.; Muchsin, N.; Ryacudu, R.; Kunto, T.; Astono, P.; Prasetya, I.; Sapiie, B.; Asikin, S.; Harsolumakso, A.H.; Yulianto, I. The Collision of the East Java Microplate and Its Implication for Hydrocarbon Occurrences in the East Java. In Proceedings of the Indonesian Petroleum Association, Jakarta, Indonesia, 14–16 October 2003.
32.  Kadarusman, A.; Massonne, H.J.; Van Roermund, H.; Permana, H.; Munasri, P.-T. Evolution of Eclogites and Blueschists from the Luk Ulo Complex of Central Java, Indonesia. *Int. Geol. Rev.* **2007**, *49*, 329–356. [CrossRef]
33.  Miyazaki, K.; Sopaheluwakan, J.; Zulkarnain, I.; Wakita, K. A Jadeite-Quartz-Glaucophane Rock from Karangsambung, Central Java, Indonesia. *Isl. Arc* **1998**, *7*, 223–230. [CrossRef]
34.  Suparka, E.R. *Studi Petrologi dan Pola Kimia Komplek Ofiolit Karangsambung Utara, Luh Ulo, Jawa Tengah*; Institut Teknologi Bandung: Bandung, Indonesia, 1988; (English Abstract Is Available)
35.  Asikin, S.; Handoyo, A.; Busono, H.; Gafoer, S. *Geological Map of Indonesia: Kebumen Quadrangle, Central Java*; Pusat Penelitian dan Pengembangan Geologi: Kota Bandung, Indonesia, 1992.
36.  Condon, W.H.; Pardyanto, L.; Amin, T.C.; Gafoer, S.; Samodra, H. *Geological Map of Indonesia: Banjarnegara-Pekalongan Quadrangle, Central Java*; Pusat Penelitian dan Pengembangan Geologi: Kota Bandung, Indonesia, 1996.

37. Harsolumakso, A.H. Diabas di daerah Karangsambung, Luk Ulo, Jawa Tengah; Apakah Bentuk Kelompok Batuan Basaltik Berupa Tubuh Intrusif? In Proceedings of the Prosiding Seminar Nasional Sumberdaya Geologi, Yogyakarta, Indonesia, 20–21 September 1999. (English Abstract Is Available)
38. Harsolumakso, A.H.; Noeradi, D. Deformasi Pada Formasi Karangsambung, Di Daerah Luk Ulo, Kebumen, Jawa Tengah. *Bull. Geol.* **1996**, *26*, 45–54. (English Abstract Is Available)
39. Purwasatriya, E.B.; Gibran, A.K.; Rizki Aditama, M.; Waluyu, G. Sedimentologi Dan Tektonostratigrafi Formasi Halang Di Cekungan Banyumas Serta Potensinya Untuk Reservoir Hidrokarbon. *J. Geol. Dan Sumberd. Miner.* **2021**, *22*, 153–163. [CrossRef]
40. Telford, W.M.; Geldart, L.P.; Sheriff, R.E. *Applied Geophysics*, 2nd ed.; Cambridge University Press: New York, NY, USA, 1990; Chapter 1, p. 16.
41. Longman, I.M. Formulas for Computing the Tidal Accelerations Due to the Moon and the Sun. *J. Geophys. Res.* **1959**, *64*, 2351–2355. [CrossRef]
42. Kane, M.F. A Comprehensive System of Terrain Corrections Using A Digital Computer. *Geophysics* **1962**, *27*, 455–462. [CrossRef]
43. Nagy, D. The Prism Method for Terrain Corrections Using Digital Computers. *Pure Appl. Geophys.* **1966**, *63*, 31–39. [CrossRef]
44. Buttkus, B. *Spectral Analysis and Filter Theory in Applied Geophysics*; Springer: Berlin/Heidelberg, Germany, 2000; ISBN 978-3-642-62943-3.
45. Guillen, A.; Calcagno, P.; Courrioux, G.; Joly, A.; Ledru, P. Geological Modelling from Field Data and Geological Knowledge. Part II. Modelling Validation Using Gravity and Magnetic Data Inversion. *Phys. Earth Planet. Inter.* **2008**, *171*, 158–169. [CrossRef]
46. Calcagno, P.; Chilès, J.P.; Courrioux, G.; Guillen, A. Geological Modelling from Field Data and Geological Knowledge. Part I. Modelling Method Coupling 3D Potential-Field Interpolation and Geological Rules. *Phys. Earth Planet. Inter.* **2008**, *171*, 147–157. [CrossRef]
47. Holstein, H. Gravimagnetic Anomaly Formulas for Polyhedra of Spatially Linear Media. *Geophysics* **2003**, *68*, 157–167. [CrossRef]
48. Plouff, D. Gravity and Magnetic Fields off Polygonal Prisms and Application to Magnetic Terrain Corrections. *Geophysics* **1976**, *41*, 727–741. [CrossRef]
49. Mosegaard, K.; Tarantola, A. Monte Carlo Sampling of Solutions to Inverse Problems. *J. Geophys. Res.* **1995**, *100*, 12431–12447. [CrossRef]
50. Tenzer, R.; Sirguey, P.; Rattenbury, M.; Nicolson, J. A Digital Rock Density Map of New Zealand. *Comput. Geosci.* **2011**, *37*, 1181–1191. [CrossRef]
51. Bosch, M.; Guillen, A.; Ledru, P. Lithologic Tomography: An Application to Geophysical Data from the Cadomian Belt of Northern Brittany, France. *Tectonophysics* **2001**, *331*, 197–227. [CrossRef]
52. Stadlober, E.; Zechner, H. The Patchwork Rejection Technique for Sampling from Unimodal Distributions. *ACM Trans. Model. Comput. Simul.* **1999**, *9*, 59–80. [CrossRef]
53. Metropolis, N.; Rosenbluth, A.W.; Rosenbluth, M.N.; Teller, A.H.; Teller, E. Equation of State Calculations by Fast Computing Machines. *J. Chem. Phys.* **1953**, *21*, 1087–1092. [CrossRef]
54. Ahmady, F.N. *Kajian Gaya Berat Pada Kelompok Batuan Pra- Tersier Dan Tersier Di Kebumen Utara, Jawa Tengah*; Institut Teknologi Bandung: Bandung, Indonesia, 2018; (English Abstract Is Available).
55. Ramdhan, M.; Widiyantoro, S.; Nugraha, A.D.; Métaxian, J.P.; Rawlinson, N.; Saepuloh, A.; Kristyawan, S.; Sembiring, A.S.; Budi-Santoso, A.; Laurin, A.; et al. Detailed Seismic Imaging of Merapi Volcano, Indonesia, from Local Earthquake Travel-Time Tomography. *J. Asian Earth Sci.* **2019**, *177*, 134–145. [CrossRef]
56. Ardianto, A.; Nugraha, A.D.; Afif, H.; Syahbana, D.K.; Sahara, D.P.; Zulfakriza, Z.; Widiyantoro, S.; Priyono, A.; Rosalia, S.; Saepuloh, A.; et al. Imaging the Subsurface Structure of Mount Agung in Bali (Indonesia) Using Volcano-Tectonic (VT) Earthquake Tomography. *Front. Earth Sci.* **2021**, *9*, 619587. [CrossRef]